Joint traveltime, waveform and waveform envelope inversion for the near surface imaging

Zhiyang Liu*, Jie Zhang, University of Science and Technology of China (USTC)

Summary

The first-arrival traveltimes constrain very shallow velocities, waveform envelope presents low-frequency data, and waveform itself with high-frequency data should include information of tremendous structure details. We propose a joint traveltime, waveform, and waveform envelope inversion method (JTWE) for inverting the near surface velocity structures. By inverting three types of data, we are able to recover both low-wavenumber and high-wavenumber structures and avoid the cycle-skipping problem in waveform inversion. The calculation of traveltimes and raypaths is fast. The main calculation is about waveform and waveform envelope. JTWE backward propagates both FWI residual and envelope residual simultaneously. This backward propagation strategy ensures that the computational cost of JTWE is reduced to the cost of inverting waveform alone. We demonstrate the effectiveness of JTWE by applying the method to both synthetics and field data.

Introduction

Full waveform inversion (FWI) has gone through tremendous research and development efforts (Tarantola, 1984; Pratt et al., 1998). However, FWI convergence tends to be uncertain when low-frequency component is absent in the data. Wu et al. (2014) extract the low-frequency component from data by accessing the envelopes of the waveforms for FWI. Inverting envelope data is able to recover the low-wavenumber model component and improve the convergence of FWI. Liu and Zhang (2015) combine that with the first-arrival traveltime tomography, and introduce a joint traveltime and waveform envelope inversion method (JTE) for near-surface imaging. JTE utilizes the first-arrival traveltime information to constrain the top model information and uses the waveform envelope information to obtain the background velocity. It can be used as a method to produce a reliable starting model for FWI to invert the near surface velocity model.

The main limitation of the above workflows is the additional computational cost for the convergence of a waveform-based inversion calculation for the waveform envelope before FWI is applied. Therefore, we propose a joint traveltime, waveform and waveform envelope inversion method (JTWE). We also use the first-arrival traveltimes to offer top model information and waveform envelope to present low-frequency data. Furthermore, we include waveform itself in the objective function and backward propagate both FWI residual and envelope residual

simultaneously. Therefore, JTWE directly recovers both low-wavenumber model components and high-wavenumber model components with a computational cost equivalent to inverting waveform alone.

Envelope data

Following Wu et al. (2014), we extract the waveform envelope by taking the amplitude after analytic signal transform using the Hilbert transform. A signal having no negative-frequency components is called an analytic signal $\tilde{\mathbf{f}}(t)$, if it is constructed from a real signal $\mathbf{f}(t)$ and its transform $\mathbf{H}\{\mathbf{f}(t)\}$:

$$\tilde{\mathbf{f}}(t) = \mathbf{f}(t) + i\mathbf{H}\{\mathbf{f}(t)\} \tag{1}$$

The envelope $\mathbf{e}(t)$ of $\mathbf{f}(t)$ can be derived by:

$$\mathbf{e}(t) = \sqrt{\mathbf{f}^2(t) + \mathbf{H}^2\{\mathbf{f}(t)\}} \tag{2}$$
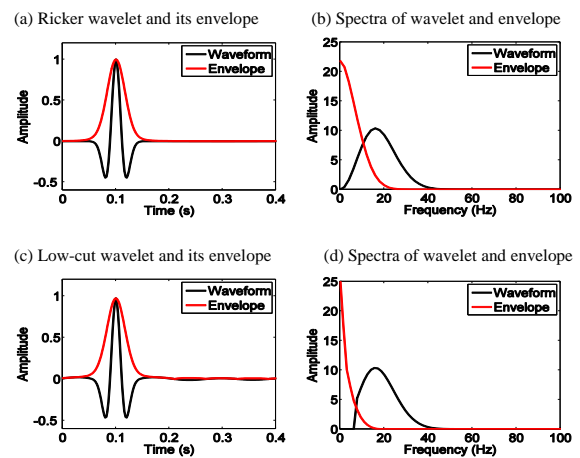

Figure 1: (a) Ricker wavelet and its envelope (black: wavelet, red: wavelet's envelope); (b) spectrum of the Ricker wavelet and its envelope spectrum (black: wavelet, red: wavelet's envelope); (c) Ricker wavelet without low frequency and its envelope (black: wavelet, red: wavelet's envelope); (d) spectrum of the Ricker wavelet without low frequency and its envelope spectrum (black: wavelet, red: wavelet's envelope).

To test the ability of waveform envelope in retrieving low frequency from seismic waveform, Ricker wavelet signals and their envelopes are plotted in Figure 1. We use two types of Ricker wavelets: one is a full-band wavelet, and the other is a low-cut wavelet (cut from 5 Hz below). Figure 1(a) and (c) show both full-band and low-cut Ricker wavelets (black

SEG International Exposition and 87th Annual Meeting

Joint Traveltime, Waveform and Waveform Envelope Inversion

lines) and their envelopes (red lines) in time domain. The corresponding waveform spectra (black lines) and envelope spectra (red lines) are plotted in Figure 1(b) and (d). We observe strong low-frequency components, but relatively weak high-frequency components from envelope spectrum shown in Figure 1(b). Even when we filter the data below 5 Hz out from the original wavelet, we can clearly observe the abundant low-frequency information in envelope spectrum from Figure 1(d).

Joint inversion algorithm

The objective function for joint traveltime, waveform and waveform envelope inversion can be imposed as follows:

$$\mathbf{\Phi}(\mathbf{m}) = \frac{1}{2} \{(1-w_1-w_2)\left\|\mathbf{e}_o^2 - \mathbf{e}_c^2(\mathbf{m})\right\|^2 + w_1\left\|\mathbf{u} - \mathbf{y}(\mathbf{m})\right\|^2 \quad (3)$$
$$+ w_2\left\|\mathbf{t}_o - \mathbf{t}_c(\mathbf{m})\right\|^2 + \alpha\left\|\mathbf{L}(\mathbf{m}-\mathbf{m}_0)\right\|^2\}$$

where $\mathbf{e}_o$ is observed waveform envelope data, $\mathbf{e}_c$ is calculated waveform envelope data, $\mathbf{u}$ is observed waveform, $\mathbf{y}$ is calculated waveform, $\mathbf{t}_o$ is picked traveltime, $\mathbf{t}_c$ is calculated traveltime, $\mathbf{m}$ is the velocity model, $\mathbf{m}_0$ is a priori model, $\mathbf{L}$ is a Laplacian operator for Tikhonov regularization, w_1 and w_2 are two weighting factors among waveform misfit, waveform envelope misfit and traveltime misfit.

To utilize waveform envelope information, we should extract envelope function from the waveform data using Hilbert transform (Wu et al., 2014; Liu and Zhang, 2015). Therefore, Equation (3) can be written as:

$$\mathbf{\Phi}(\mathbf{m}) = \frac{1}{2}\{(1-w_1-w_2)\left\|(\mathbf{y}^2+\mathbf{y}_H^2)-(\mathbf{u}^2+\mathbf{u}_H^2)\right\|^2$$
$$+ w_1\left\|\mathbf{u}-\mathbf{y}(\mathbf{m})\right\|^2 + w_2\left\|\mathbf{t}_o-\mathbf{t}_c(\mathbf{m})\right\|^2 + \alpha\left\|\mathbf{L}(\mathbf{m}-\mathbf{m}_0)\right\|^2\} \quad (4a)$$
$$= \frac{(1-w_1-w_2)}{2}\left\|\mathbf{E}\right\|^2$$
$$+ \frac{w_1}{2}\left\|\mathbf{u}-\mathbf{y}(\mathbf{m})\right\|^2 + \frac{w_2}{2}\left\|\mathbf{t}_o-\mathbf{t}_c(\mathbf{m})\right\|^2 + \frac{\alpha}{2}\left\|\mathbf{L}(\mathbf{m}-\mathbf{m}_0)\right\|^2$$

$$\mathbf{E} = (\mathbf{y}^2+\mathbf{y}_H^2)-(\mathbf{u}^2+\mathbf{u}_H^2) \quad (4b)$$

where $\mathbf{u}_H$ and $\mathbf{y}_H$ are corresponding Hilbert transforms, and $\mathbf{E}$ is the instant envelope data residual.

We apply a nonlinear conjugate gradient method to minimize the above objective function, and calculate the following gradient that will determine the model update direction:

$$\frac{\partial\mathbf{\Phi}(\mathbf{m})}{\partial\mathbf{m}} = 2(1-w_1-w_2)\mathbf{F}^T\mathbf{P} + w_1\mathbf{F}^T\mathbf{Q} \quad (5a)$$
$$- w_2\mathbf{A}^T(\mathbf{t}_o-\mathbf{t}_c(\mathbf{m})) + \alpha\mathbf{L}^T\mathbf{L}(\mathbf{m}-\mathbf{m}_0)$$

$$\mathbf{F} = \frac{\partial\mathbf{y}(\mathbf{m})}{\partial\mathbf{m}} \quad (5b)$$

$$\mathbf{P} = \mathbf{E}^T\mathbf{y} - H(\mathbf{E}^T\mathbf{y}_H) \quad (5c)$$

$$\mathbf{Q} = \mathbf{y}(\mathbf{m})-\mathbf{u} \quad (5d)$$

where $\mathbf{P}$ is the backward propagation wavefield for envelope inversion that provides with sensitivity impact for low-wavenumber component (Wu et al., 2014; Liu and Zhang, 2015), $\mathbf{Q}$ is the backward propagation wavefield for waveform inversion part, and $\mathbf{A}$ is a sensitivity matrix of traveltimes containing raypath information, equivalent to the impact of traveltime sensitivity. It should be noted that envelope inversion part and waveform inversion part share the same forward propagation matrix $\mathbf{F}$. We then utilize it to reduce the computational burden.

To obtain a cost-effective gradient, we rearrange Equation (5a) under the objective function pattern of JTE (Liu and Zhang, 2015):

$$\frac{\partial\mathbf{\Phi}(\mathbf{m})}{\partial\mathbf{m}} = (1-w_2)\mathbf{F}^T[\frac{2(1-w_1-w_2)\mathbf{P}}{1-w_2}+\frac{w_1\mathbf{Q}}{1-w_2}]$$
$$- w_2\mathbf{A}^T(\mathbf{t}_o-\mathbf{t}_c(\mathbf{m}))+\alpha\mathbf{L}^T\mathbf{L}(\mathbf{m}-\mathbf{m}_0) \quad (6a)$$
$$= (1-w_2)\mathbf{F}^T\mathbf{P}_s - w_2\mathbf{A}^T(\mathbf{t}_o-\mathbf{t}_c(\mathbf{m}))+\alpha\mathbf{L}^T\mathbf{L}(\mathbf{m}-\mathbf{m}_0)$$

$$\mathbf{P}_s = \frac{2(1-w_1-w_2)}{1-w_2}[\mathbf{E}^T\mathbf{y}-H(\mathbf{E}^T\mathbf{y}_H)]+\frac{w_1}{1-w_2}[\mathbf{y}(\mathbf{m})-\mathbf{u}]$$
$$(6b)$$

The Equation (6a) can be implemented by zero-lag correlation of the forward propagated source wavefield $\mathbf{F}$ and the backward propagated residual wavefield $\mathbf{P}_s$ (Tanrantola, 1984; Pratt et al., 1998; Wu et al., 2014). The backward propagated residual wavefield $\mathbf{P}_s$ contains both envelope residual for low-wavenumber recovery and waveform residual for high-wavenumber recovery. It benefits JTWE because both forward propagation and backward propagation only need to be calculated once for every iteration. Thus, the computational cost of JTWE for one iteration is reduced to the same level of JTE.

We also design a weighting-factor setting strategy. We add a damping parameter between waveform inversion part and waveform envelope inversion part, so that we run joint traveltime and envelope inversion in the beginning to build

Joint Traveltime, Waveform and Waveform Envelope Inversion

up the low-wavenumber structure, and end up with joint traveltime and waveform inversion to recover the details.

Nonlinearity

To illustrate the nonlinearity of various objective functions fitting different types of data, we use a constant velocity model to calculate the objective functions analytically. These include fitting traveltimes, waveform envelope, waveform, and joint traveltime, waveform and waveform envelope. The true model is homogenous with a velocity of 2000 m/s. The synthetic data includes a shot at the surface, and 100 receivers with receiver spacing of 25 m. The central frequency of the data is 11 Hz. The objective functions for velocities varying from 500 to 3500 m/s with an interval of 50 m/s are calculated and shown in Figure 2.
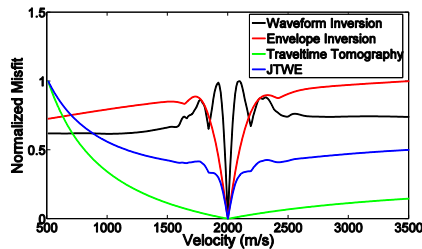

Figure 2: Objective functions for different near-surface inversion strategies (black: waveform inversion, red: envelope inversion, green: first-arrival traveltime tomography, blue: JTWE)

Figure 2 depicts that the waveform objective function clearly includes more local minima than others. The traveltime objective function is the simplest with one global minima for a single velocity model. But it also shows the least sensitivity to the solution which corresponding to the low resolution. The envelope objective function improves the curve for fitting waveform, but still showing some variations associated with local minima. The joint traveltime, waveform and waveform envelope inversion seems improving the objective function toward to a single global minimum. It suggests that joint traveltime, waveform and waveform envelope inversion can mitigate the dependence of initial model better than FWI. Therefore, we combine waveform envelope and nonlinear traveltime inversion, and take advantages of the two methods for recovering low-wavenumber model components in near-surface area. Also, we include waveforms for the high-wavenumber model components to refine the structure details.

Synthetic tests

We test the accuracy and efficiency of our approach using a synthetic dataset. This data is generated from a model with a low-velocity inclusion, as shown in Figure 3. A stand-alone first-arrival traveltime tomography (Zhang and Toksoz, 1998) or FWI without low-frequency data may fail to

recover such models if a starting model is too far. The data are modeled assuming 70 shots with 50 m spacing and a low-cut Ricker wavelet with the peak frequency of 10 Hz (cut from 5Hz below). Also, the wavefield is recorded by 140 receivers with 25 m spacing.
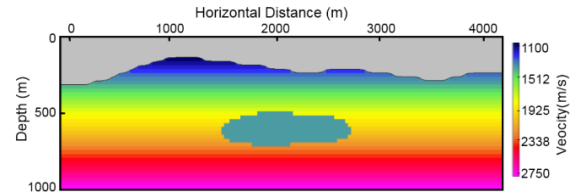

Figure 3: The true model with a low-velocity inclusion.

To demonstrate the convergence efficiency achieved by JTWE, we show the reduction of waveform residuals with iterations (Figure 4) and compare it to JTE+FWI workflow. JTE iterates 25 times for this dataset. And then FWI is applied using JTE result as an input model (also 25 iterations). Compared with JTE+FWI workflow (black line), JTWE (red line) converges to the same level of waveform residuals within 25 iterations.

The model results are shown in Figure 5. As we expected, first-arrival traveltime tomography after 10 iterations gives a result (Figure 5(a)) which fails to recover the low-velocity inclusion. It leads FWI to fall into a local minimum which corresponds to a poor model solution (Figure 5(d)). It clearly demonstrates the failure of FWI to estimate the low-wavenumber components of the velocity model. In contrast, FWI successfully reveals the low-velocity inclusion with the help of low-wavenumber recovery by JTE (Figure 5(b)). Figure 5(c) shows the model solution using JTWE. It also recovers low-velocity inclusion just as the more expensive JTE+FWI workflow.
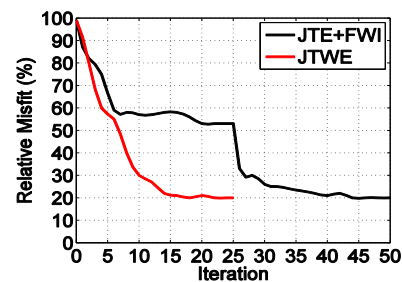

Figure 4: Reduction of waveform residuals with iterations. Comparison of JTE+FWI workflow (black line) and JTWE (red line).

Field data applications

We apply the above method to field data on a 2D line. This

Joint Traveltime, Waveform and Waveform Envelope Inversion

dataset includes 558 shots with interval of 60 m, and about 240 receivers for each shot with interval of 30 m. We pick first-arrival traveltimes from field records manually. The average reciprocal error associated with the picked time is around 6 ms. To obtain an initial model for proposed method, we apply a first-arrival traveltime tomography to yield the initial model (Figure 6).

(a) The traveltime tomography result

(b) The inverted model of JTE+FWI

(c) The inverted model of JTWE

(d) FWI solution using traveltime tomography result as input
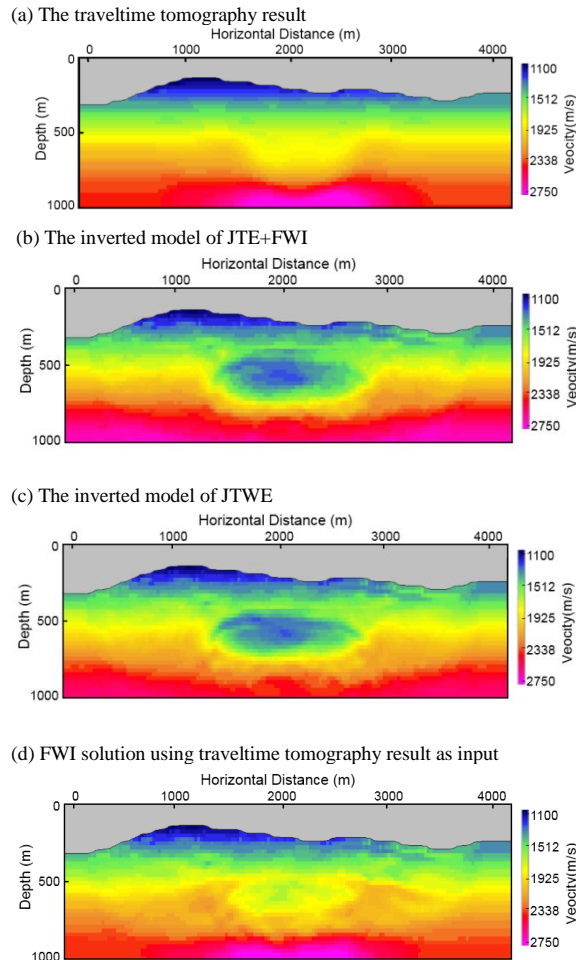

Figure 5: (a) The traveltime tomography result; (b) the inverted model of joint traveltime and waveform envelope inversion; (c) the inverted model of FWI using the joint inversion result as an input model; (d) the inverted model of FWI using traveltime tomography result as an input model.

Figure 7 depicts the inversion results from this field data using both FWI and JTWE. Both methods use traveltime tomographic solution as an input model. Overall, the relative deep area shows similar velocities to the first-arrival traveltime tomography result, but the top near-surface area of both methods further varies. To be specific: in Figure 7(a), the arrows indicate the areas where FWI solution departs

from the traveltime tomographic solution and produce lower velocity. However, in Figure 7(b), our approach clearly brings that back.
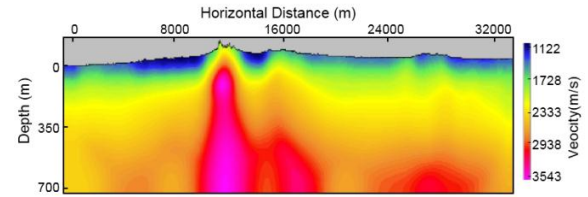

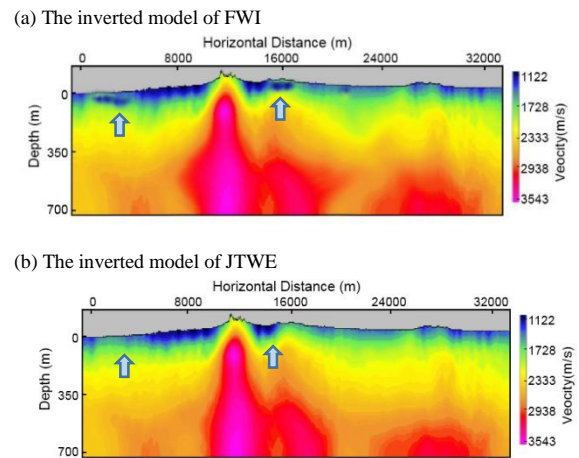Figure 6: The first-arrival traveltime tomography result using data on a 2D line.

(a) The inverted model of FWI

(b) The inverted model of JTWE

Figure 7: Comparison of model solutions between two methods: (a) the inverted model of FWI; (b) the inverted model of JTWE.

Conclusions

We develop a joint traveltime, waveform and waveform envelope inversion (JTWE) method for the near surface imaging. This approach offers an effective algorithm to invert for both low-wavenumber and high-wavenumber structures in the near-surface area. It utilizes traveltimes to constrain the top velocity structure, uses waveform envelope for low-wavenumber model recovery and waveform for detailed structure information. Also, JTWE reduces the computational cost by backward propagating both FWI residual and envelope residual simultaneously. The synthetic tests and application to field data further show the feasibility and efficiency of the approach for solving a near-surface imaging problem.

Acknowledgments

We appreciate the support of GeoTomo, for allowing us to use the TomoPlus software package for this study.

REFERENCES

Liu, Z., and J. Zhang, 2015, Joint traveltime and waveform envelope inversion for near-surface imaging:
    Presented at the 84th Annual International Meeting, SEG, Expanded Abstracts, 1154–1158,
    http://dx.doi.org/10.1190/segam2015-5863259.1.

Pratt, R. G., C. Shin, and G. J. Hicks, 1998, Gauss-Newton and full Newton methods in frequency-space
    seismic waveform inversion: Geophysical Journal International, **133**, 341–362,
    http://dx.doi.org/10.1046/j.1365-246X.1998.00498.x.

Tarantola, A., 1984, Inversion of seismic-reflection data in the acoustic approximation: Geophysics, **49**,
    1259–1266, http://dx.doi.org/10.1190/1.1441754.

Wu, R. S., J. Luo, and B. Wu, 2014, Seismic envelope inversion and modulation signal model:
    Geophysics, **79**, no. 3, WA13–WA24, http://dx.doi.org/10.1190/geo2013-0294.1.

Zhang, J., and J. Chen, 2014, Joint seismic traveltime and waveform inversion for near surface imaging:
    Presented at the 84th Annual International Meeting, SEG, Expanded Abstracts, 934–937,
    http://dx.doi.org/10.1190/segam2014-1501.1.

Zhang, J., and M. N. Toksoz, 1998, Nonlinear refraction traveltime tomography: Geophysics, **63**, 1726–
    1737, http://dx.doi.org/10.1190/1.1444468.